Romanian Reports in Physics, Vol. 65, No. 4, P. 1390–1397, 2013

CHARACTERIZATION OF THERMIONIC VACUUM ARC DEPOSITED Co-MgF_2 GRANULAR THIN FILMS USING X-RAY DIFFRACTION AND MICROSCOPY TECHNIQUES*

V. IONESCU[1], C.P. LUNGU[2], I. JEPU[2], M. OSIAC[3], G.E. IACOBESCU[3]

[1] "Ovidius" University, Department of Physics and Electronics, 900527, Constanta, Romania
E-mail: ionescu.vio@gmail.com
[2] National Institute for Laser, Plasma and Radiation Physics, Bucharest-Magurele, 077125 Romania
[3] University of Craiova, Faculty of Physics, 200585, Craiova, Romania

Received July 12, 2012

Abstract. The paper presents the synthesis of Co-MgF_2 granular films deposited by the thermionic vacuum arc technique, with the simultaneous ignition of plasma in Co and MgF_2 vapors, respectively. Transmission electron microscopy (TEM) and X-Ray diffraction (XRD) investigations revealed the microstructure of the films. The surface morphology of the samples was analyzed by using the power spectral density (PSD) function and the root-mean-square (RMS) roughness obtained from the atomic force microscopy (AFM) data.

Key words: termionic vacuum arc, rougnness, power spectral density.

1. INTRODUCTION

Metal/insulator granular systems composed of grains of a ferromagnetic element (such as Fe, Co, or Ni) immersed in an insulating matrix have been extensively studied in the last few years, mainly because they can present unique magnetotransport properties that make them good candidates for future technological applications. For example, Co-MgF_2 granular system is used as thin film inductor in power converters for microprocessors, with fast response, high efficiency and small size [1, 2].

The electronic transport in these systems is believed to be determined by spin-dependent tunneling [3–6], networks of magnetic tunnel junctions being formed between neighboring ferromagnetic dots.

The present study promotes a novel deposition technique called thermionic vacuum arc (TVA) [7] for deposition of smooth, nanostructured Co-MgF_2 granular thin films.

* Paper presented at the 8th General Conference of Balkan Physical Union, July 5–7, 2012, Constanţa, Romania.

In this paper, we analyzed the morphological and the structural properties of this type of films, evaporated onto two type of substrate: glass and silicon. We selected magnesium fluoride as insulating material because it is easy to be evaporated, has the propensity to separate from a co-evaporated metal, and has high resistivity due to the wider band gap and smaller dielectric constants than MgO and Al_2O_3.

2. EXPERIMENTAL

Thermionic vacuum arc (TVA) method employed here for the granular coatings deposition and described in detail elsewhere [8] was based on the use of two electron beams emitted by two externally heated cathodes of W with the diameters of 1 mm; the beams, accelerated by high anodic voltages, are bombarding simultaneously the depositing materials (Co and MgF_2) placed in crucibles (anodes), which will be intensely evaporated. Applying high voltages (1-6 kV) between cathodes and anodes, two plasmas in vapors of pure Co and MgF_2 ions were formed in the high vacuum chamber (the pressure inside the chamber being $< 2\times10^{-5}$ torr); the plasma expands further in the neighborhood high vacuum space, where the grounded substrates for sample preparation were mounted. Due to the high energy dissipated in the unit volume plasma, the material was strongly dispersed and completely droplets free.

The experimental arrangement for the obtaining of Co-MgF_2 granular films is presented in Fig.1, where it must be mentioned that the concentration of the magnetic metal in the MgF_2 dielectric matrix will expectedly decrease continuously with x (for $x < L$), due to the different distances of the substrates to the two anode positions.

The film substrates were 15×15 mm^2 rectangular pieces of industrial glass and silicon ordered on two lines. The thin film samples investigated were P_1 and P_2 probes placed at the mid-distance (21.1 cm) between the anodes. The distance between the Co crucible and samples was 25 cm. The substrates were maintained at $T = 300$ K during deposition.

The intensity of the TVA current and voltage for the discharge in Co vapors was $I_{disch} = 0.7–0.8$ A and $U_{disch} = 400$ V; in the case of the discharge in MgF_2 vapors, those values were $I_{disch} = 0.4–0.5$ A and $U_{disch} = 300–400$ V respectively. Deposition rate r_d and film thickness d were measured and controlled *in situ* using a FTM7 quartz microbalance. The thickness of the Co-MgF_2 coatings was 200 nm.

Transmission Electron Microscopy (TEM) analysis were carried out by a Philips CM120ST microscope operating at 100 kV with $C_s = 1{,}2$ mm and ≈ 2 Å resolution.

The X-ray diffraction (XRD) patterns were obtained using a Shimadzu model 600 thin film diffractometer operating with Cu Kα radiation (45 kV, 40 mA).

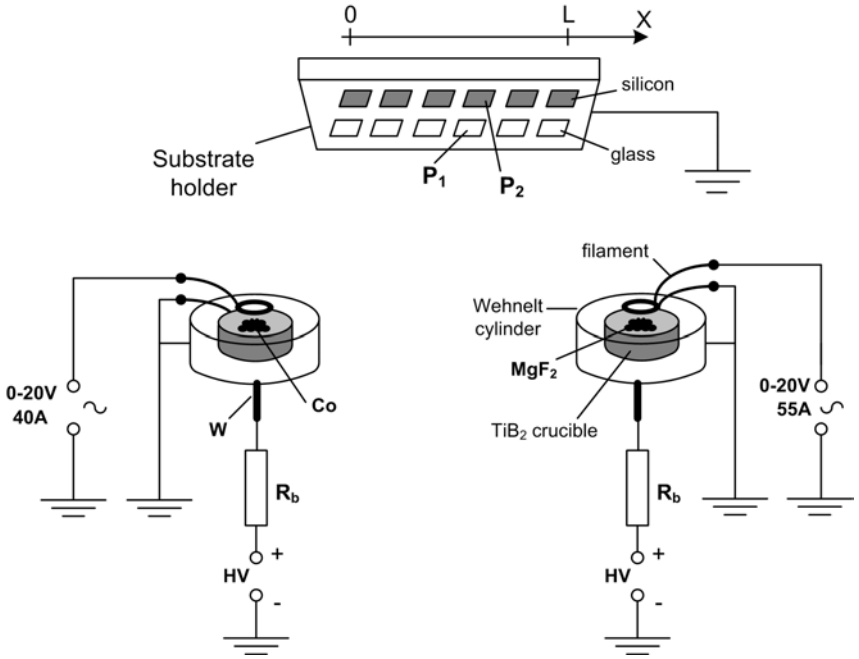

Fig. 1 – The experimental set-up for Co-MgF_2 thin film deposition.

The atomic force microscopy (AFM) data were recorded in non-contact mode using a Park XE-100 equipment (silicon tip with conical shape).

The topographical AFM images in combination with a a subsequent statistical data analysis, including the calculation of the RMS roughness and power spectral density (PSD) analysis gave detailed information about the surface morphology.

3. RESULTS AND DISCUSSIONS

The TEM image of P_1 sample presented in Fig. 2 shows the presence of some very fine dark spots (Co) fixed in a lighter area surface (MgF_2), indicating the granular nanostructure of the film.

Low-angle XRD analyses were performed to establish the presence of crystalline phases in the coatings. In the XRD patterns of both samples P_1 and P_2 the 2θ diffraction peaks can be assigned to (110), (111), (210), (211) and (310) crystalline planes of MgF_2 tetragonal phase (Fig. 3). No crystalline phase for Co was observed in these spectra, concluding that the Co crystals in MgF_2 matrix have random orientation.

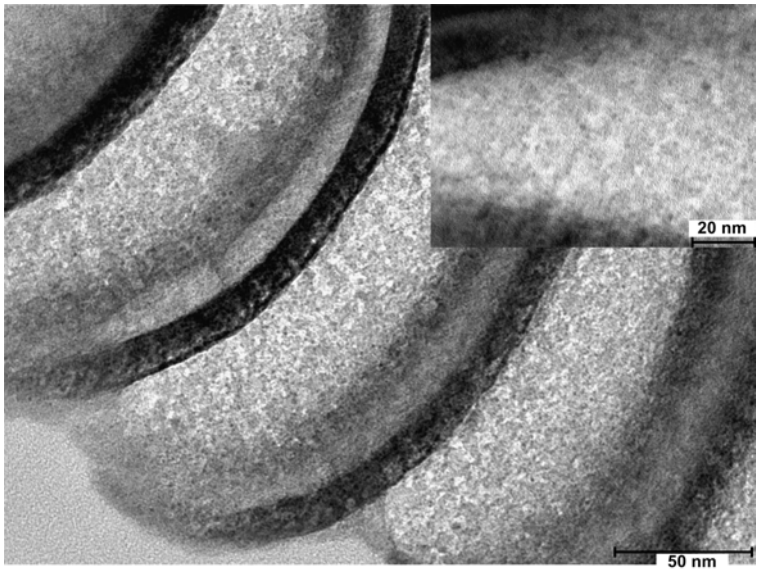

Fig. 2 – Cross-sectional TEM images for P_1 sample.

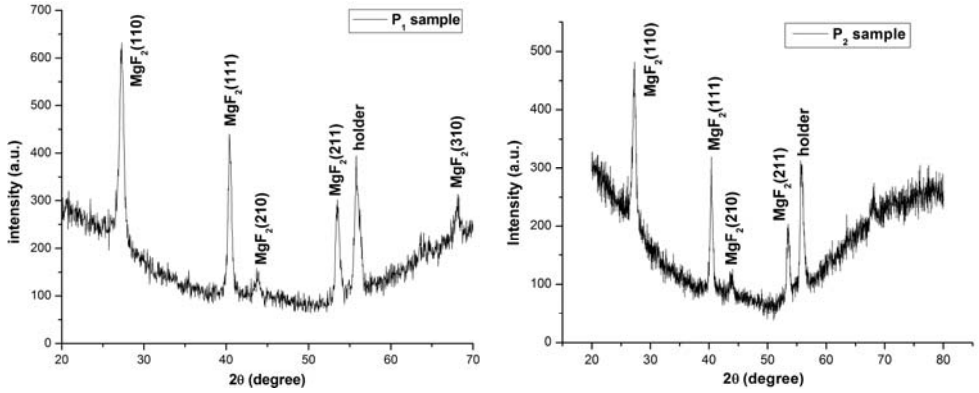

Fig. 3 – XRD patterns of P_1 and P_2 samples.

The simplest and most common method used for the observation of changes in surface topography is called the root mean square (RMS) roughness calculation, based on finding a median surface level for the image and then evaluating the standard deviation within the image. The equations for the determining de 1D and 2D surface roughness are [9, 10]:

$$R_{q1D} = \sqrt{\frac{1}{N}\sum_{n=1}^{N}(H_n - \bar{H})^2}\,, \tag{1}$$

$$R_{q2D} = \sqrt{\frac{1}{N^2}\sum_{i=1}^{N}\sum_{j=1}^{N}(H(i,j)-\bar{H})^2}\,, \tag{2}$$

where H_n is the deposit height at point n, i and j are the pixel locations on the AFM image, $\bar{H}$ is the average value of the height across the entire image and N is the number of data points in the image (AFM images are typically stored as 256×256 or 512×512 data arrays). The primary limitations of this algorithm are that makes no distinction between peaks and valleys and does not show the lateral spacing of various surface features.

Spanos and Irene [11] demonstrated the fact that three calculated cosine functions with different frequencies and amplitudes yield identical RMS roughness values even though these three surfaces would be very different due to the difference in spatial frequency of the surface features.

Power Spectral Density (PSD) is a technique that calculates power (roughness amplitude squared) as a function of spatial frequencies of the features that are contributing to the surface images [12]. PSD analysis is based on a Fast Fourier Transform (FFT) algorithm, which separates the original waveform of AFM profile in its constituent sine waveforms. The PSD gives the power of each of these constituent waveforms and allows analyzing which frequencies occur most often and import the greatest influence to the surface topography. Smaller surface features will have a higher spatial frequency. More details about FFT and PSD can be found in [13–15].

In order to increase the frequency range of the resulting PSD areas, we presented here PSD curves obtained from combined AFM results, which were recorded over scan areas of 2×2 μm^2 and 10×10 μm^2.

AFM 2D images of P_1 sample morphology are presented in Fig. 4, showing a surface with a few irregularities and no uniform grains being observed here. In the PSD curve showed under the image and taken after a 2×2 μm^2 scan of the sample, we observed two basic peaks (of 3.5×10^{-7} μm^4 and 4×10^{-7} μm^4), at the spatial frequencies of about 1 μm^{-1} and 2 μm^{-1}, respectively. The most intense peak in the PSD curve corresponding to 10×10 μm^2 surface scanning of this probe (Fig. 4b) has the value of about 3×10^{-5} μm^4, being present at a spatial frequency under 1 μm^{-1}. RMS Rq roughness values calculated for P_1 sample where 4.2 nm for 2×2 μm^2 scan area and 7.1 nm for 10×10 μm^2 scan area.

For the P_2 probe deposited on silicon substrate, AFM images from Fig. 5 showed morphology with grains that are uniformly distributed over the surface. This sample presented grain size diameter varying in the range of 10–100 nm.

From the PSD curves presented in Fig. 5a we could see that there were a lot more spatial frequencies, with peaks located at over 2.5 μm^{-1} which influence the surface topography; the important peaks of those curves (of about 10^{-8} μm^4), located at higher frequencies than in the case of P_1 sample, indicated clearly the smaller morphological features of this sample.

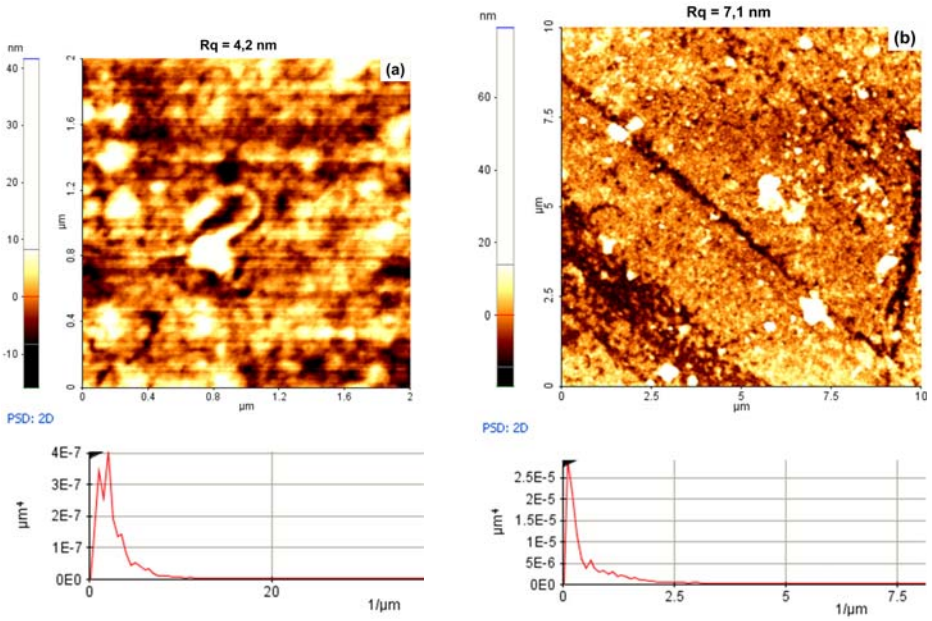

Fig. 4 – AFM top view images and PSD curves for: a) 2 × 2 µm^2; b) 10 × 10 µm^2 scan areas of P_1 sample surface (glass substrate).

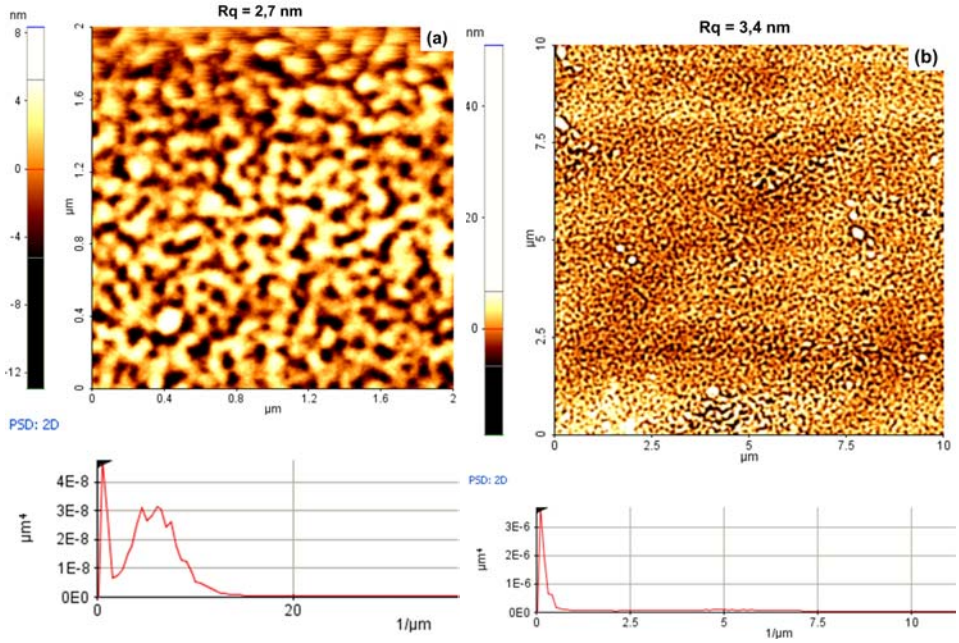

Fig. 5 – AFM top view images and PSD curves for: a) 2 × 2 µm^2; b) 10 × 10 µm^2 scan areas of P_2 sample surface (on silicon substrate).

RMS Rq roughness values calculated for P_1 sample where 2.7 nm and 3.4 nm, respectively.

AFM topographical images from Fig. 6 were characterized by slight surface roughness with uniform crack-free, densely packed microstructure. The in-plane size of the surface asperities of the P_1 sample (see Fig. 6a) was almost uniform for the scanning area investigated, just a small number of those asperities being beyond 10 nm in height.

From the 3D AFM image presented in Fig. 6b for the P_2 sample, we have seen a very smooth surface with uniform asperities of about 4 nm in height.

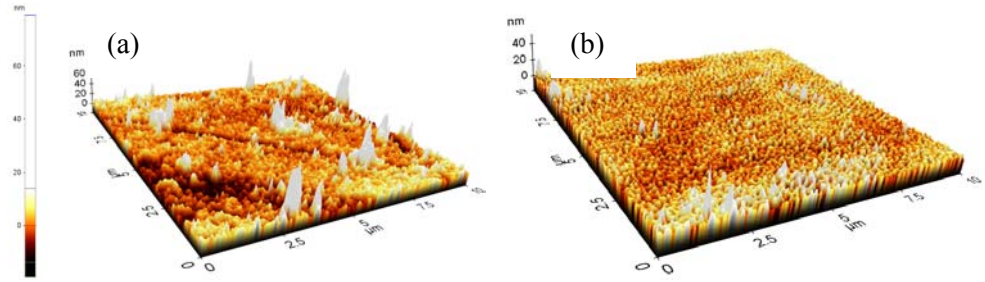

Fig. 6 – AFM 3D digital maps images for 10 × 10 μm^2 scan area of the samples: a) P_1; b) P_2.

H. Hosoya *et al.* [16] reported in the case of Fe-SrF_2 co-evaporated granular films on MgO substrates, surfaces with asperities having in-plane size of several tens on nanometers, some asperities being much more than 10 nm in height.

4. CONCLUSIONS

The Co-MgF_2 granular thin films with the thickness of about 200 nm were successfully deposited onto silicon and glass substrates using the TVA method.

XRD and TEM investigations showed the presence of crystalline phase of MgF_2 in the nanostructured films with granular features.

From AFM measurements, we observed a Co-MgF_2 sample deposited on silicon substrate with uniformly distributed grain morphology and surface asperities under 4 nm in height; this probe presented the smaller Rq roughness values (2–3nm), giving also the lowest values (10^{-8} μm^4) for different PSD peaks registered at frequencies up to 10 μm^{-1}, in comparison with the sample deposited on glass substrate with high PSD peaks (10^{-6} μm^4) for frequencies under 2.5 μm^{-1}.

So, we can conclude with high accuracy that the silicon substrates are more proper for the deposition of some very smooth Co-MgF_2 films, with small roughness features.

Acknowledgements. This work was supported by a grant of the Romanian National Authority for Scientific Research, CNCS – UEFISCDI, project number PN-II-ID-PCE-2011-3-0522.

REFERENCES

1. C. R. Sullivan and S. R. Sanders, IEEE Trans. Power Electronics, **11**, 228 (1996).
2. K.D. Coonley, G.J. Mehas, C.R. Sullivan, U.J. Gibson, IEEE Transactions and Magnetics, **36,** 3463 (2000).
3. H. Fujimori, S. Mitani and S. Ohnuma, Mater. Sci. Eng. B, **3**, 219 (1995).
4. A. Milner, A. Gerber, B. Groisman, M. Karporsky and A. Gladkikh, Phys. Rev. Lett., **76**, 475 (1996).
5. Y. Hayakawa, N. Hasegawa, A. Makino, S. Mitani and H. Fujimori, J. Magn. Magn. Mat., **154**, 175 (1996).
6. I. Mustata, C. P. Lungu, A. M. Lungu, V. Zaroski, M. Blideran and V. Ciupina, *Vacuum*, **76,** 131 (2004).
7. C. P. Lungu, I. Mustata, G. Musa, A. M. Lungu, V. Zaroschi, K. Iwasaki, R. Tanaka, Y. Matsumura, I. Iwanaga, H. Tanaka, T. Oi and K. Fujita, Surf. and Coat. Techn., **200**, 399 (2005).
8. G. Musa, I. Mustata, M. Blideran, V. Ciupina, R. Vladoiu, G. Prodan and E. Vasile, J. Optoelectron. Adv. Mater., **5**, 667 (2003).
9. J.D. Kiely and D.A. Bonnel, J. Vacuum Sci. and Technol. B, **15**, 1483 (1997).
10. J. Morales, S.M. Krijer, P. Esparza, S. Gonzales, L. Vasquez, R.C. Salvarezza and A.J Arvia, Langmuir, **12**, 1068 (1996).
11. L. Spanos and E.A. Irene, J. Vacuum Sci. and Technol. A **12**, 2646 (1994).
12. S.J. Fang, S. Haplepete, W. Chen, C.R. Helms and H. Edwards, J. Appl. Phys., **82**, 5891(1997).
13. J.M. Elson and J.M. Bennett, Applied Optics, **34**, 201 (1995).
14. C. Ruppe and A. Duparre, Thin Solid Films, **288**, 8 (1996).
15. J.K. Lawson, C.R.Wolfe, K.R. Manes, J.B. Trenholme, D.M. Aikens and R.E. English Jr., Proc. SPIE, **2536**, 38(1995).
16. H. Hosoya, M. Arita, K. Hamada, Y. Takahashi, K. Higashi, K. Oda, M. Ueda, Journal of Physics D: Applied Physics, **39**5, 1039 (2006).